ISSN 0915-633X

NATIONAL INSTITUTE FOR FUSION SCIENCE

Stimulated Photon Cascade and Condensate in Relativistic Laser-plasma Interaction

K. Mima, M.S. Jovanović, Y. Sentoku, Z-M. Sheng,
M.M. Škorić and T. Sato

(Received - Nov. 6, 2000)

NIFS-669 Nov. 2000

RESEARCH REPORT
NIFS Series

TOKI, JAPAN

Invited Lecture presented at 42nd Annual Meeting of the APS Division of Plasma Physics combined with the 10th International Congress on Plasma Physics, October 23-27, 2000, Quebec City, Canada

Stimulated photon cascade and condensate in relativistic laser-plasma interaction

K. Mima[1], M.S. Jovanović[1], Y. Sentoku[1], Z-M. Sheng[1], M.M. Škorić[2] and T. Sato[2]

[1]) *Institute of Laser Engineering, Osaka University, Suita, Osaka*

[2]) *Theory and Computer Simulation Center, National Institute for Fusion Science, Toki, Gifu*

Abstract

The propagation of a linearly polarized relativistic laser pulse in an underdense plasma is studied by fluid-Maxwell and PIC simulations. A nonlinear interplay between backward and forward stimulated Raman scattering instabilities produces a strong spatial modulation of the light pulse and the down-cascade in its frequency spectrum. The Raman cascade saturates by a unique photon condensation at the bottom of the light spectra near the electron plasma frequency, related to strong depletion and possible break-up of the laser beam. In the final stage of the cascade-into-condensate mechanism, depleted downshifted laser pulse is gradually transformed into a train of ultra-short relativistic light solitons.

KEYWORDS: plasma turbulence, laser interactions, relativistic plasmas, fast ignition

1 Introduction

Ever since much acclaimed paper of Akhiezer and Polovin [1] plasma theorists have been attempting to comprehend complex dynamics related to the propagation of high and ultra-high intensity electromagnetic (EM) radiation through a plasma. This topic was successfully revisited a number of years later by Kaw and Dawson [2] whose analysis threw more light on the propagation of coupled longitudinal-transverse waves of arbitrary intensities. The very high phase velocity case was solved exactly soon by Max and Perkins [3]. The problem of relativistic laser-plasma interactions is of particular interest concerning the fast ignitor concept [4], relevant to contemporary inertial confinement fusion research. Moreover, understanding of relativistic laser pulse evolution in a plasma is basic to many new applications, including optical-field-ionized x-ray lasers [5], plasma-based electron accelerator schemes [6], as well as to interpretation of some astrophysical phenomena. Most of the above applications require relativistic or channel guiding of laser beams over longer distances, without significant energy losses. The pioneer workers in this field [1, 2, 3] did not consider the stability of the plane-wave solutions related to nonlinear interaction between normal plasma modes. This illustrates all the complexity of the posed problem, even the propagation of a single plane-wave appears intractable, and we have to deal with nonlinearly coupled modes under various plasma conditions.

Linearly polarized relativistic EM radiation sets plasma electrons into the longitudinal motion by the strong $\mathbf{v}\times\mathbf{B}$ forces changing its nature to a coupled longitudinal-transverse mode. So are also one-dimensional (1D) electron parametric instabilities: stimulated Raman forward- and backward-scattering (F-SRS and B-SRS, respectively) and relativistic modulational instability (RMI). They do not appear isolated, but always coupled with other instabilities [7, 8]. This paper will mostly discuss F-SRS and B-SRS induced by picosecond mod-

erate to high intensity laser pulses in long length-scale plasmas. Particular attention will be paid to effects of their mutual interplay and couplings to RMI. This results in rich 1D- dynamics reflected in spectral broadening and cascading process which transfers the incident laser energy to higher order scattering modes. Along the propagation beam, there is typically a cascade in the light spectrum from fundamental (laser) frequency toward lower frequencies. The first Stokes line is significant, however, further with laser propagation it becomes a new pump which decays via a secondary Raman scattering. This cascade process is halted around the plasma frequency, the cut-off frequency for light propagation. We find that continuing instability growth through stimulated Raman cascade downshifts a maximum from the fundamental to the bottom of the light spectra. This unique stimulated photon condensation following a Raman cascade, appears as a striking example of the relativistic laser instabilities. This is similar to a situation with the Langmuir condensate in a weak Langmuir turbulence theory [9, 10], where a condensate is due to a Langmuir decay spectral cascading down to small wavenumbers

When making a comparison between homogeneous temporal growth rates of B-SRS and F-SRS in a weakly relativistic case, we conclude that their ratio is roughly $(n_e/n_c)^{-3/4}$, where n_c is the critical density, which means that the Raman backscatter growth time is 5-30 times shorter than its forward-scatter counterpart when plasma density is varied from 0.1nc to 0.01nc. However, it should be noted that B-SRS gets saturated efficiently at very early stage of evolution while that F-SRS and RMI can get close and even merge to a unique F-SRS/RMI instability, which competes with the B-SRS instability in the process of anomalous absorption of laser energy.

All mentioned processes have been intensively studied by theory and simulations [11, 12, 13, 14]. Unfortunately, due to the difficulties related to nonlinear electron dynamics and anharmonicity in the plasma response, linearly polarized as compared to circularly polarized light has received less theoretical consideration. So, in the present paper our attempt to solve a fully nonlinear system of cold electron-fluid and Maxwell equations for 1D-propagation of high-intensity linearly polarized laser light in a uniform underdense plasma is presented. We also check the conclusions by a 1D and 2D particle-in-cell (PIC) simulations. The PIC method can follow the evolution of the laser light and plasma waves and particles on short time scales, much less than the laser period.

The paper is organized as follows. In Section II. relativistic fluid-Maxwell code is described and typical results are presented. while Sec. III gives some results of PIC simulations for the parameter domain same as above. Finally, in Sec. IV the results of both methods are compared. Particular attention is paid on spectral characteristics of the propagating laser pulse, followed by a discussion on the spectral Raman cascade and condensation of the laser beam energy to the bottom of the light spectrum, leading in its final stage to generation of relativistic solitons.

2 Relativistic fluid-Maxwell model

A long laser pulse enters the plasma and propagates in the x-direction, inducing both transverse and longitudinal electron motion. We consider only a purely one-dimensional case, in which the EM field is described by longitudinal (E_x) and transverse (E_y) electric field components and magnetic field B_z. For further treatment it is convenient to normalize all the physical quantities to dimensionless values by introducing light-speed units. We express length x in $c\omega_0^{-1}$ and time t in ω_0^{-1}-units, and normalize electron fluid velocity v, momentum p, fields E and B, vector potential A and density n_e to c, mc, $mc\omega_0 e^{-1}$, $m\omega_0 e^{-1}$, mce^{-1} and n_0, respectively. Here c, m, e, ω_0 and n_0 designate vacuum speed of light, electron mass and (absolute) charge, laser light frequency and initial homogeneous electron density, respectively. In this way Maxwell equations reduce to

$$\frac{\partial E_x}{\partial t} = \frac{n_e p_x}{\gamma}, \tag{1}$$

$$\frac{\partial E_y}{\partial t} + \frac{\partial B_z}{\partial x} = \frac{n_e A}{\gamma}, \tag{2}$$

$$\frac{\partial B_z}{\partial t} + \frac{\partial E_y}{\partial x} = 0, \tag{3}$$

$$\frac{\partial A}{\partial t} = -E_y, \tag{4}$$

while cold electron fluid quantities are described by the continuity and electron motion equations:

$$\frac{\partial n_e}{\partial t} = -\frac{\partial}{\partial x}\left(\frac{n_e p_x}{\gamma}\right), \tag{5}$$

$$\frac{\partial p_x}{\partial t} = -E_x - \frac{\partial \gamma}{\partial x}, \tag{6}$$

where $\gamma = (1+p_x^2+A^2)^{1/2}$, and transverse momentum p_y is substituted by the vector potential component A under the Coulomb gauge; with an immobile neutralizing ion background assumed. Unlike

the small amplitude case (weak pump case and linear stability analysis) in the strong-pump limit considered here, the only exact analytical solution of the system of equations (1)-(6) can be tailored for circularly polarized EM pump. Direct numerical solving of the above system has not been performed often in the past [16]. So, our effort has been put into a building of a stable numerical scheme for solving the 1D system (1)-(6) in a fully nonlinear form, without any approximations. The fluid equations were treated by the second-order accuracy Lax-Wendroff method. As for the EM fields, a kind of a central scheme of a leap-frog type was applied with simultaneous calculation of all values assisted by averaging exact electric and magnetic fields to approximate mesh node values at every space and time step. Surprisingly, the instability switch-on time was perfectly independent of the initial noise in the present simulation. The explanation of this effect lies in the fact that $\mathbf{v}\times\mathbf{B}$-induced longitudinal motion serves as a seed for instability development.

In order to conclude about the backward- and forward-scattering properties: reflectivity R and transmittivity T are introduced:

$$R(x,t) = (F^-)^2/E_0^2 \quad T(x,t) = (F^+)^2/E_0^2, \quad (7)$$

where F^+ and F^- are forward- and backward-propagating combined EM fields in a plasma

$$F^{\pm}(x,t) = E_y \pm B_z \quad (8)$$

3 Results and discussion

We have studied a propagation of a rather long, high-intensity laser pulse with a relative intensity a_0 varied within the interval 0.1-1.0, where

$$a_0 = eE_0/m\omega_0 c \approx 8.5\times 10^{-6} I^{1/2}\lambda_0 W^{-1/2} \quad (9)$$

So, roughly speaking, the intensity range $10^{16} - 10^{18}\mathrm{Wcm}^{-2}$ was covered for laser light of 1μm in wavelength. Plasma was initially uniform in density, with $n_0 = 0.1n_c$ in most considered cases. The pulse was typically about 1ps in length (several hundred vacuum laser periods) or more, long enough to induce various electron parametric instabilities, including forward and backward Raman and relativistic modulational instability and to follow their competition and nonlinear interplay and saturation. The front of the pulse is initially smoothed by a parabolic function to avoid extremely high ponderomotive action ahead of the pulse, which could easily destabilize the numerical procedure.

For lower pump intensities ($a_0 = 0.1$) stimulated Raman scattering in a linear regime occurs, with Stokes component in the frequency spectrum far dominant over anti-Stokes one (Fig. 1). Along the propagating beam, there is a cascade in the light spectrum from fundamental (laser) frequency toward lower frequencies. The first Stokes line is significant, however, along the propagation, the Stokes mode further decays via a secondary Raman scattering. This cascade process is eventually halted near the electron plasma frequency - the cut-off for the light propagation. Further the laser intensity a_0 was raised to the value of 0.2. Although still moderately relativistic, typically, a strong modulation, depletion and breakup of the pulse take place (Fig. 2). This effect is well-known from earlier simulations with ultra- intense ultra-short laser pulses [12, 13, 14, 15]. Although initially with the higher growth rate, the predominantly convective B-SRS instability (in the pulse frame) stops its temporal growth to saturate over a short distance from the pulse front. Such strong backscattering depletes the pulse energy locally creating a sort of a notch at some position in the laser pulse [15]. However, this erosion in the body of the pulse will not significantly affect the F-SRS, which although with a moderate growth rate (typically $(n_e/n_c)^{-3/4}$ times smaller than that of B-SRS) will develop at each point inside the pulse producing a considerable modulation for practically any laser intensity.

To establish a connection to previous studies on stimulated Raman scattering in preformed underdense plasmas, we look at the time evolution of the reflectivity R (Fig. 3). Figs. 3a,b show the SRS reflectivity vs. time for two pump intensities ($a_0 = 0.2$ and 0.3), while Figs. 3c,d give the time-integrated reflected energy to estimate the total fraction of the laser energy (about 1/10 of its input value in these simulations). Further, we compare these results with 1D-PIC simulation data for the same parameters (Figs. 3e,f). We note a high degree of agreement between the two methods applied. Nonetheless, it is clear that the major fraction of input energy goes to forward-scattered and plasma wave modes and into electron heating, the latter not being captured by the Fluid model. Moreover, the experimental and computational evidence indicates that even an underdense plasma can be a source of accelerated MeV-electrons [17]. Considering the B-SRS spectra obtained from 1D-PIC code (Fig. 4) we observe interesting features pointing to their general character. The B-SRS spectra taken for $a_0 = 0.2$ and $a_0 = 0.3$ at the plasma boundary ($x = 0$) reveal the tendency of cascading laser energy to lower-frequency spectral modes. The continuing instability growth through Raman cascade downshifts the F-SRS maximum

from the fundamental to the bottom of the light spectra. This unique stimulated photon condensation following the Raman cascade, appears as a striking example of the relativistic laser instabilities. Such behavior is also confirmed by our fluid simulation (Fig. 5) showing also that the energy cascade-into-condensate gets more pronounced with increasing laser intensity. As emphasized above, the B-SRS instability is also responsible for a reflection of the relatively small fraction of the input energy. Moreover, the cascade scenario was checked upon again on the example of F-SRS which is, obviously, more important concerning the amount of laser energy converted into the forward scattered modes. In Fig. 6 we show the F-SRS spectra for two pump values: $a_0 = 0.2, 0.3$. It is clear that in F-SRS anti-Stokes scattered modes also carry a finite amount of laser energy. With increasing pump intensity a_0 we again observe a strong cascade-into-condensate channel of the laser energy down conversion.

For sustained intense pumping ($\sim a_0 > 0.5$) the photon energy density at the condensate further accumulates and grows (see Fig. 7 for $a_0 = 1$). In this regime, abrupt transition to space-time chaos and breaking of plasma and light waves is typically found, resulting in turbulent broadened frequency and wavenumber spectra. This behavior is related to an onset of chaos, predicted in the simple B-SRS model with nonlinear relativistic plasmon-phase shift [18]. As confirmed in the present simulations, the accompanying effect is the catastrophic laser pulse breakup, which becomes more apparent in recent 2D particle simulations [15, 19]. For the relativistic intensity $a_0 = 1$ in Fig. 7, unlike some of the previous examples, the fundamental line is well kept in the spectrum. This is due to the fact that at high laser intensities SRS declines in relation to the moderately relativistic case (Figs. 4-6). The Fig. 7 also re-confirms a pretty good agreement between Fluid-Maxwell and PIC code results.

In order to check the generality of the observed stimulated scattering properties we applied the 2D-PIC simulations in a simulation box $200\lambda_0 \times 50\lambda_0$ filled with a cold uniform plasma of the density $n_e = 0.1n_c$, with $12.5\lambda_0$-vacuum layers on both sides in the laser propagation direction. In Fig. 8 the 2D-profile of the laser pulse energy density (averaged over the laser period T_0) is plotted for three subsequent times during the pulse propagation. Futhermore, Fig. 9 gives a view of the frequency spectrum of the transmitted light variation across the outgoing plasma boundary (bottom), together with the spectral intensity distribution on the central axis (top). These spectra clearly reveal the linear Raman-cascade containing both the first anti-Stokes and first and second Stokes modes, which are later to evolve into a strong photon condensate (see Fig. 6 e.g.). The already mentioned break-up of the body of the laser pulse appears here again; moreover at almost the same position and time as in fluid simulations. A strong spatial self-modulation of the order of $2\pi c/\omega_p$ ($\sim 3\lambda_0$) corresponding to F-SRS/RMI instability is observed already at an early stage of 2D- propagation. The similar effect on the laser energy, showing intense spiky modulation of the pulse front followed by a strongly depleted pulse region, is evident also in 1D-fluid simulations (Figs. 10a,b). The wavenumber (k) spectra offer a better insight into the peculiarities of the spatial variation and their consequences. The k-spectra of the electric field at the moment $t = 200T_0$ for two different laser intensities are given in Fig. 11. The case in Fig. 11a ($a_0 = 0.3$) reveals the initial stage of cascading with clear discrete spectra, to be later developed into a turbulent photon condensate at very low k-values (Fig. 11b, for $a_0 = 0.4$. This picture confirms our conjectures about the high relevance of the cascade-into-condensate mechanism in relativistic laser-plasma interaction.

The finding that the Raman cascade gets saturated via the photon condensation mechanism, bears a similarity with a situation with the Langmuir condensate in a weak Langmuir turbulence theory [9, 10]. In the latter case, a condensate is due to a Langmuir decay spectral cascading down to small wavenumbers. As no dissipation exists at long wavelengths a uniform random plasmon state can become modulationally unstable, described in its nonlinear stage by the Zakharov model, a generalized type of the nonlinear Schroedinger equation. The latter possesses the stable 1D Langmuir soliton solutions which are likely to collapse in 2D and 3D cases, becoming a basic building block of the theory of Strong Langmuir turbulence. Indeed for a photon condensate, in the laser pulse frame, one can also derive the NLSE which is modulationally unstable leading to a generation of relativistic EM solitons coupled with density depressions [20, 21, 22]. Accordingly, the photon turbulence at the condensate, in the presence of the depleted pump, is expected to be modulationally unstable, nonlinearly saturating to localized 1D soliton-like light structures, as reported in some earlier analytical and PIC simulation studies [20, 22]. Another possibility also exists for solitons to be directly generated from the spikes nucleated in density depressions as a result of nonlinear F- SRS and RMI (vide supra) [23]. This might be a reason

for predominantly observing the solitons with the width of the order of F-SRS-RMI lengths. Indeed, a possibility of soliton generation in relativistic interactions has been confirmed in the simple case of our 1D-fluid cold electron plasma simulations (Fig. 12). In Fig. 12, for two different laser intensities ($a_0 = 0.3$ and 0.5) we find a fine evidence of relativistic solitons formed in the final stage of the cascade-into-condensate saturation of the laser pulse. As already noticed in Fig. 10, a spiky, spatially modulated pulse front travels with a group velocity related to an unperturbed laser pulse. The front is followed by a strongly depleted downshifted body of the laser pulse, in a process of relativistic saturation. The solitons are born from the localized light spikes in the wake of the strongly depleted front edge of the laser pulse. They begin to lag behind the pulse front, to eventually form a remarkable pattern of the standing soliton light-structures, sometimes, slowly moving in the backward direction [19, 22]. Further along the propagation path, the energy of the strongly depleted downshifted laser pulse gets gradually transformed into a train of ultra-short light solitons. It is evident that each relativistic soliton is trapped inside the local self-consistent electron density cavity, produced by a steep gradient of the relativistic ponderomotive force, as illustrated in Fig.13.

4 Summary

We have investigated the propagation of a linearly polarized relativistic laser pulse in an underdense plasma by 1D Fluid-Maxwell as well as 1D and 2D PIC simulations. While the circular polarization was earlier studied in detail, a case of a more realistic linear polarization has received much less attention. A nonlinear interplay between backward and forward stimulated Raman scattering and relativistic modulational instabilities is found to produce a strong spatial modulation of the laser pulse and the down-cascade in the light frequency spectrum. The Raman cascade nonlinearly saturates to a unique photon turbulence condensate at the bottom of the light spectra near the electron plasma frequency, corresponding to strong depletion, erosion and possible break-up of the laser beam. In the final stage of the cascade-into-condensate mechanism, depleted downshifted laser pulse gradually transforms its energy into a train of ultra-short relativistic light solitons.

Acknowledgments

M.S.J. and Z-M.S. acknowledge the research fellowship by Japan Society for Promotion of Science (JSPS). One of us (M.M.S.) is grateful for the visiting professorship granted by the Ministry of Education, Science and Culture of Japan. This work is supported in parts by Project 01E11 of the Ministry of Science and Technology of Republic of Serbia.

References

[1] A.I. Akhiezer and R.V. Polovin, Sov. Phys. JETP **3**, 696 (1956).

[2] P. Kaw and J. Dawson, Phys. Fluids **13**, 472 (1970).

[3] C. Max and F. Perkins, Phys. Rev. Lett. **27**, 1342 (1971).

[4] M. Tabak, J. Hammer, M. Glinsky, W. Kruer, S. Wilks, J. Woodworth, E.M. Campbell, M. Perry, and R. Mason, Phys. Plasmas **1**, 1626 (1994).

[5] P. Amendt, D.C. Eder, and S.C. Wilks, Phys. Rev. Lett. **66**, 2589 (1991).

[6] T. Tajima and J. Dawson, Phys. Rev. Lett. **43**, 267 (1979); A. Modena, Z. Najmudin, A. E. Dangor, C. E. Clayton, K. A. Marsh, C. Joshi, V. Malka, C. B. Darrow, C. Danson, D. Neely, and A. F. Walsh, Nature **377**, 608 (1995).

[7] S. Guerrin, G. Laval, P. Mora, J. C. Adam, A. Heron, and A. Bendib, Phys. Plasmas **2**, 2807 (1995).

[8] H.C. Barr, P. Mason, and D.M. Parr, Phys. Plasmas **7**, 2604 (2000).

[9] V.E. Zakharov, Sov. Phys. JETP **35**, 908 (1972).

[10] M.V. Goldman, Rev. Mod. Phys. **56**, 709 (1984).

[11] A.S. Sakharov and V.I. Kirsanov, Phys. Rev. E **49**, 3274 (1994).

[12] W.B. Mori, C.D. Decker, D.E. Hinkel, and T. Katsouleas, Phys. Rev. Lett. **72**, 1482 (1994).

[13] C.D. Decker, W.B. Mori, T. Katsouleas, and D.E. Hinkel, Phys. Plasmas **3**, 1360 (1996).

[14] B. Quesnel, P. Mora, J.C. Adam, S. Guerin, A. Heron, and A. Laval, Phys. Rev. Lett. **78**, 2132 (1997).

[15] K-C Tzeng, W.B. Mori, and C.D. Decker, Phys. Rev. Lett. **76**, 3332 (1996).

[16] S. Hain and P. Mulser, Laser Part. Beams **15**, 541 (1997).

[17] J.C. Adam, S. Guerin, A. Heron, and A. Laval, Phys. Rev. Lett. **84**, 3598 (2000); G. Malka, J. Fuchs, F. Amiranoff et al., Phys. Rev. Lett. **79**, 2053 (1997).

[18] S. Miyamoto, K. Mima, M.M. Škorić and M. Jovanović, J. Phys. Soc. Japan **4**, 1281 (1998); M M. Škorić, T. Sato, A Maluckov, and M.S. Jovanović, Phys Rev. E **50**, 7426 (1999).

[19] Y. Sentoku, T.Zh. Esirkepov, K. Mima et al , Phys. Rev. Lett. **83**, 3434 (1999).

[20] P.K. Kaw, A. Sen, and T. Katsouleas, Phys. Rev. Lett. **68**, 3172 (1992).

[21] H.H. Kuehl, C.Y Zhang, and T Katsouleas, Phys. Rev. E **47**, 1249 (1993).

[22] S.V. Bulanov, T.Zh Esirkepov, N.M. Naumova, F. Pegoraro, and V.A. Shivkov, Phys. Rev. Lett **82**, 3440 (1999); and references therein.

[23] D. Russel, D.F. DuBois, and H.A. Rose, Phys. Rev. Lett. **60**, 581 (1988).

Figure Captions

Figure 1: Frequency spectra of forward-propagating laser light at the points: (a) $x = 60\lambda_0$ and (b) $x = 200\lambda_0$, respectively, inside a plasma, for $a_0 = 0.1$.

Figure 2: Spatial dependence of transverse laser electric field in the fluid model for $a_0 = 0.3$, $n_e = 0.1n_c$, $T_e = 0$. A strong modulation, depletion and breakup of the pulse take place.

Figure 3: SRS reflectivity vs. time for two pump intensities: $a_0 = 0.2$ and $a_0 = 0.3$ (a,b respectively), the time-integrated values of reflected energy (c,d) and the corresponding data from 1D-PIC simulation for the same parameters.

Figure 4: B-SRS spectra (at $x = 0$) obtained from 1D-PIC code, for $a_0 = 0.2$ (a) and $a_0 = 0.3$ (b).

Figure 5: B-SRS spectra obtained from the fluid code, for $a_0 = 0.2$ (a) and $a_0 = 0.3$ (b).

Figure 6: F-SRS spectra for two pump values: (a) $a_0 = 0.2$ at $x = 100\lambda_0$ and (b) $a_0 = 0.3$ at $x = 200\lambda_0$.

Figure 7: Forward (dashed line) and backward (solid line) electromagnetic frequency spectra for laser intensity $a_0 = 1.0$, obtained from 1D-PIC simulation (a) and Maxwell-fluid simulations (b).

Figure 8: 2D-distribution of EM energy density (averaged over laser period T_0) in three time moments of the pulse propagation, as obtained from 2D-PIC simulation.

Figure 9: Transmitted light spectrum variation in transverse direction (bottom) and its spectral distribution on the axis (top), obtained in 2D PIC simulations.

Figure 10: Spatial distribution of EM energy density at (a) $t = 150T_0$ and (b) $t = 200T_0$ as obtained from 1D-Fluid simulation.

Figure 11: The k-spectra of the electric field spatial dependence at the moment $t = 200T_0$ for two different incident laser intensities: (a) $a_0 = 0.3$ and (b) $a_0 = 0.4$.

Figure 12: Spatial-temporal distribution of EM energy density between $t = 150T_0$ and $t = 400T_0$ for $a_0 = 0.3$ (a) and $a_0 = 0.5$ (b), as obtained from 1D-Fluid simulation.

Figure 13: Spatial dependence of EM energy density (a) and electron plasma density (b) at $t = 360T_0$, from 1D-Fluid simulation.

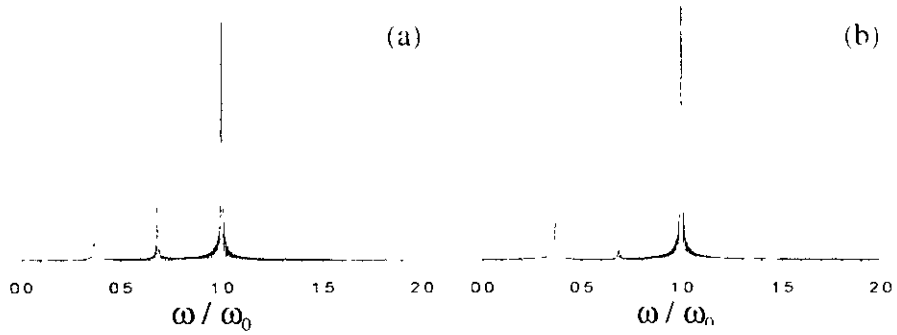

Figure 1.

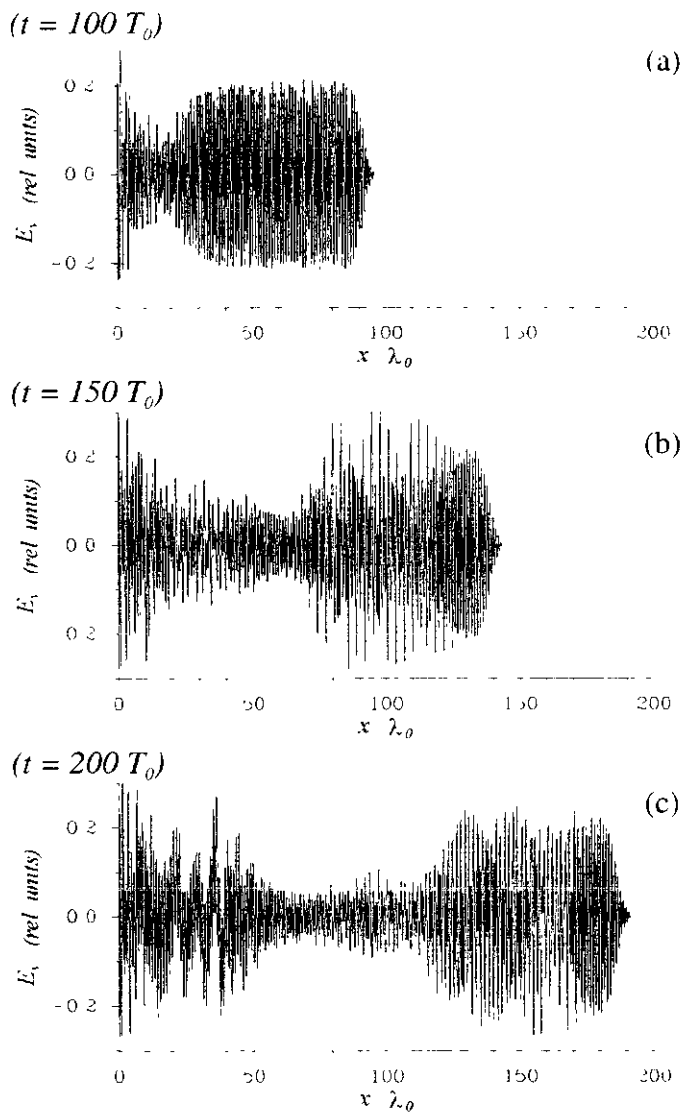

Figure 2.

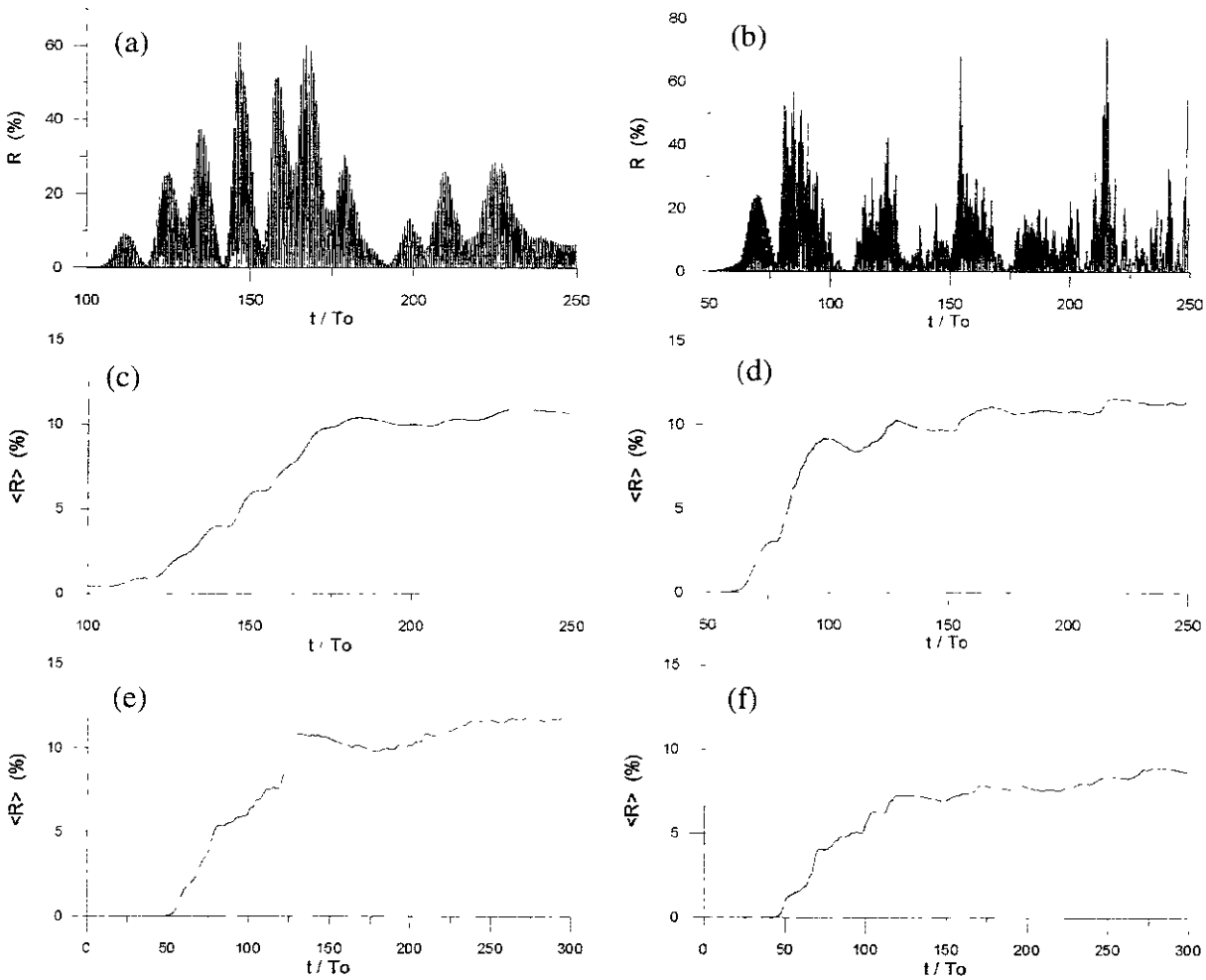

Figure 3.

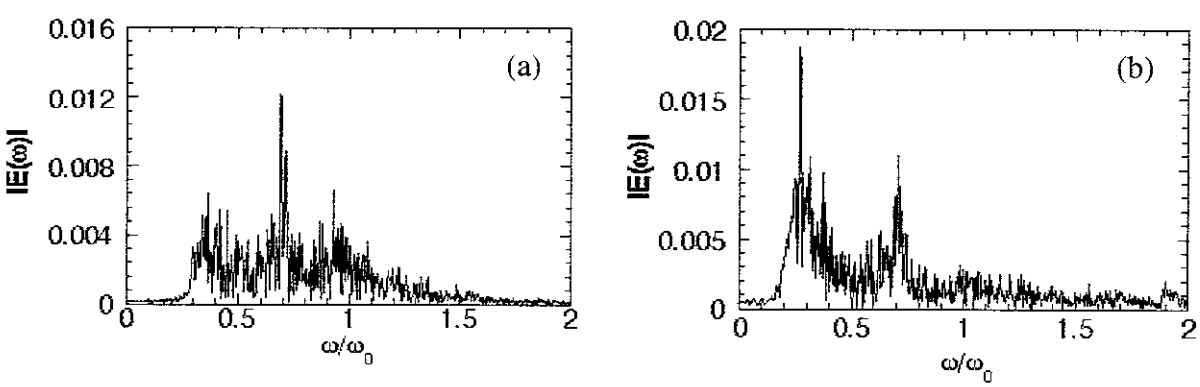

Figure 4.

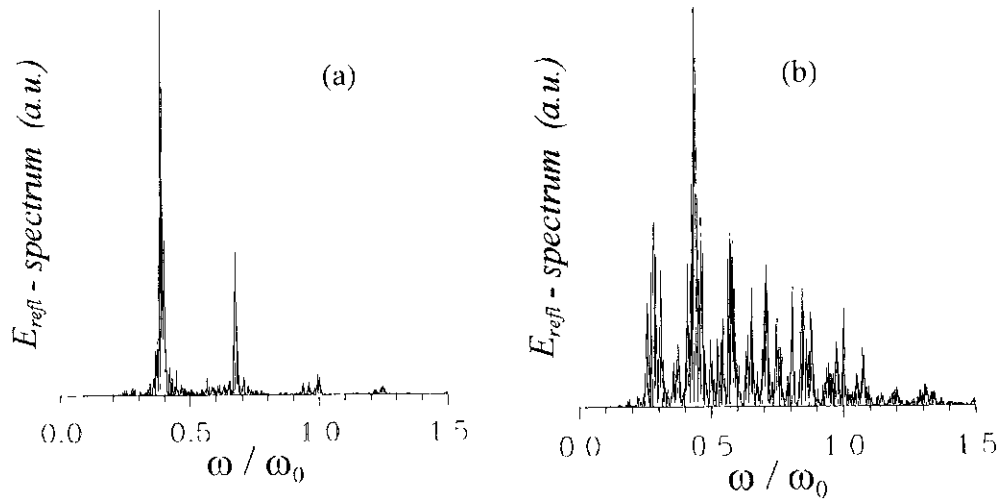

Figure 5.

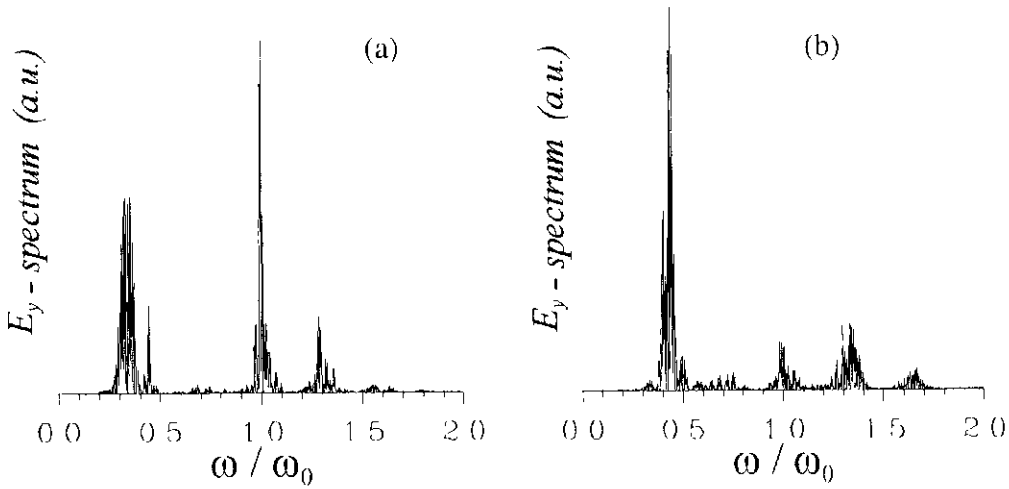

Figure 6.

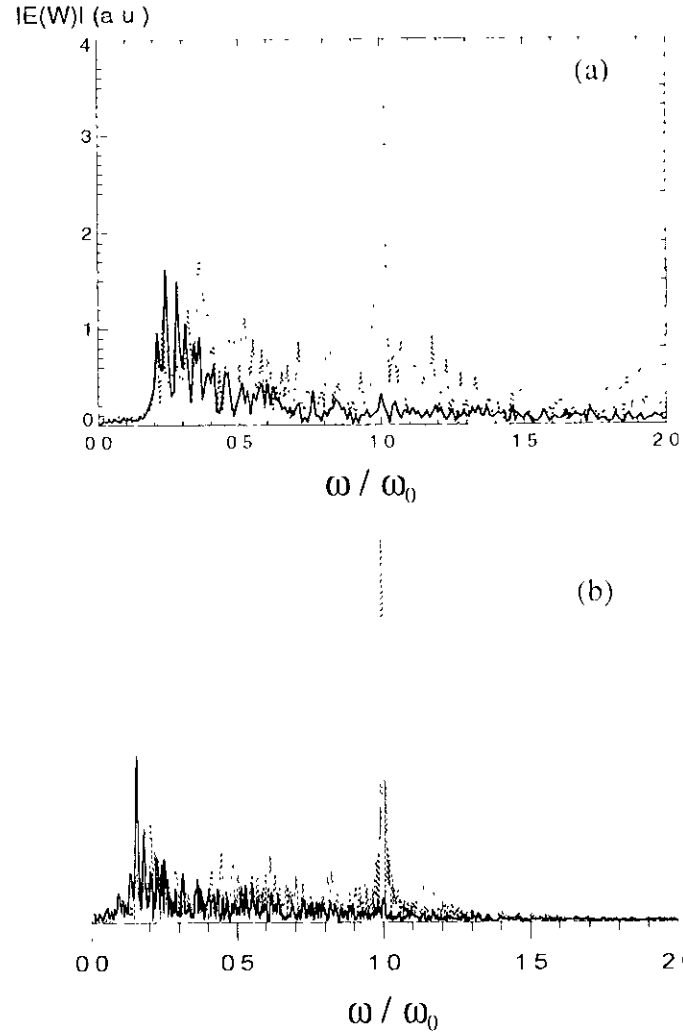

Figure 7.

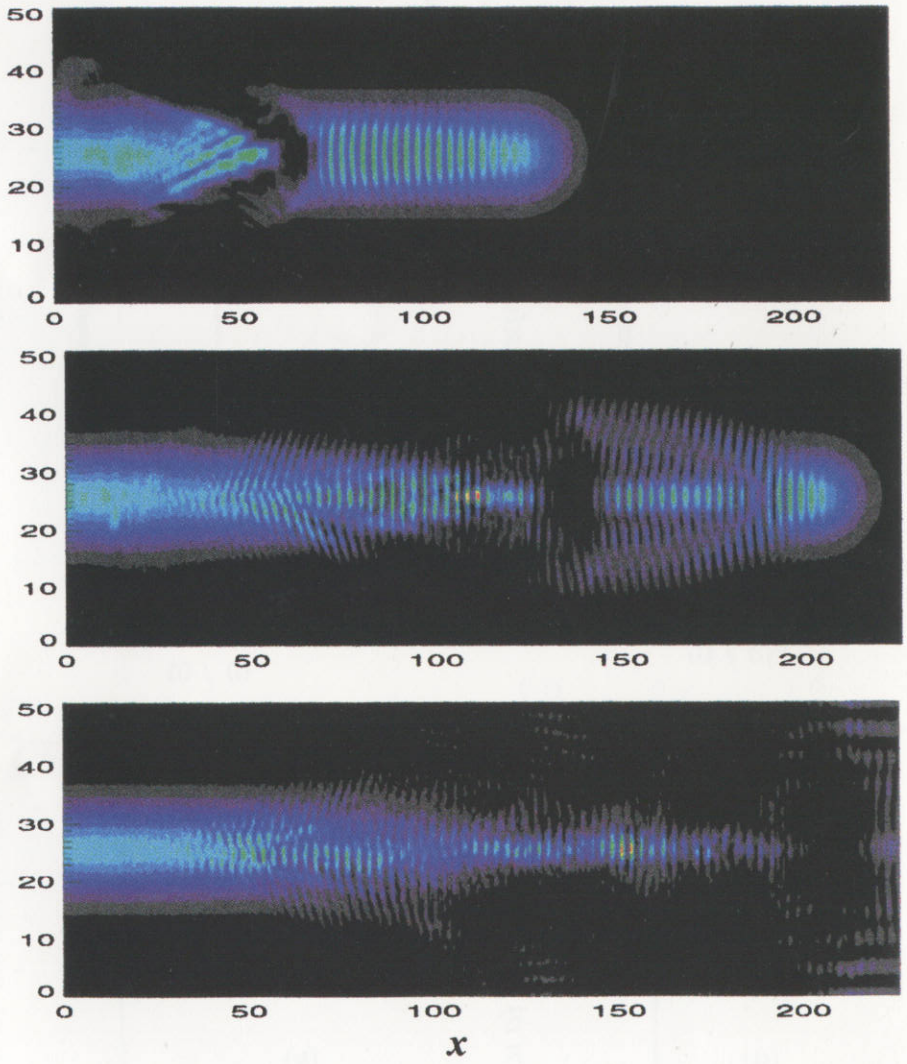

Figure 8.

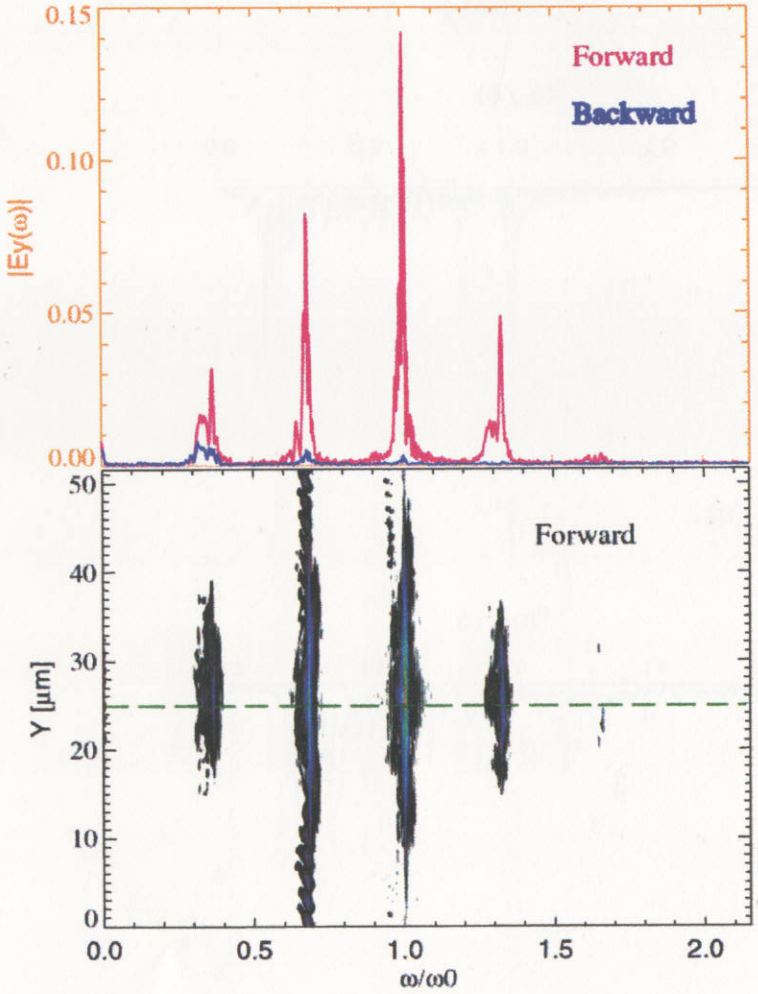

Figure 9.

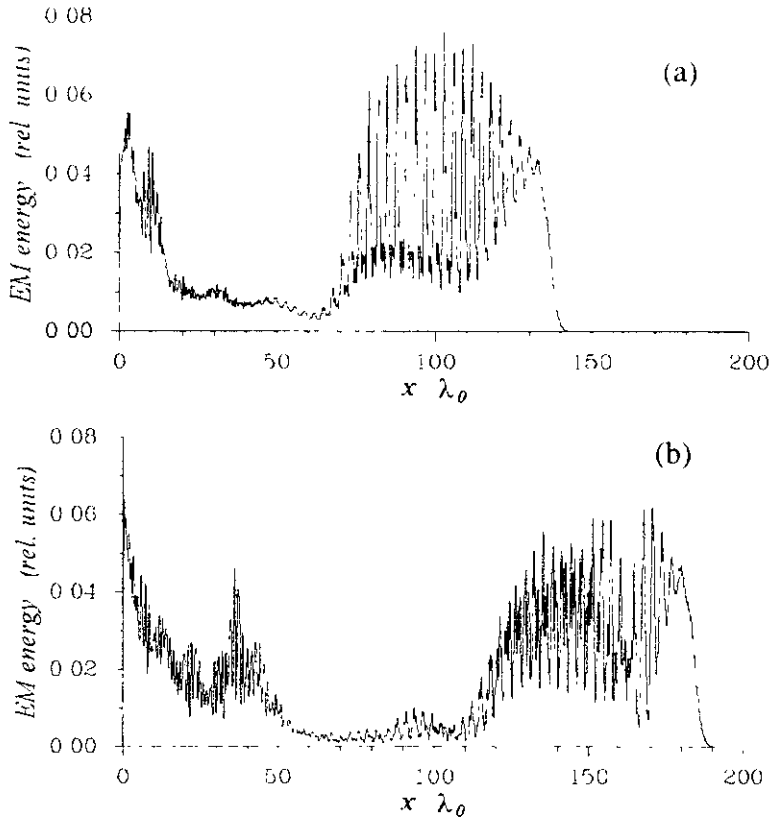

Figure 10.

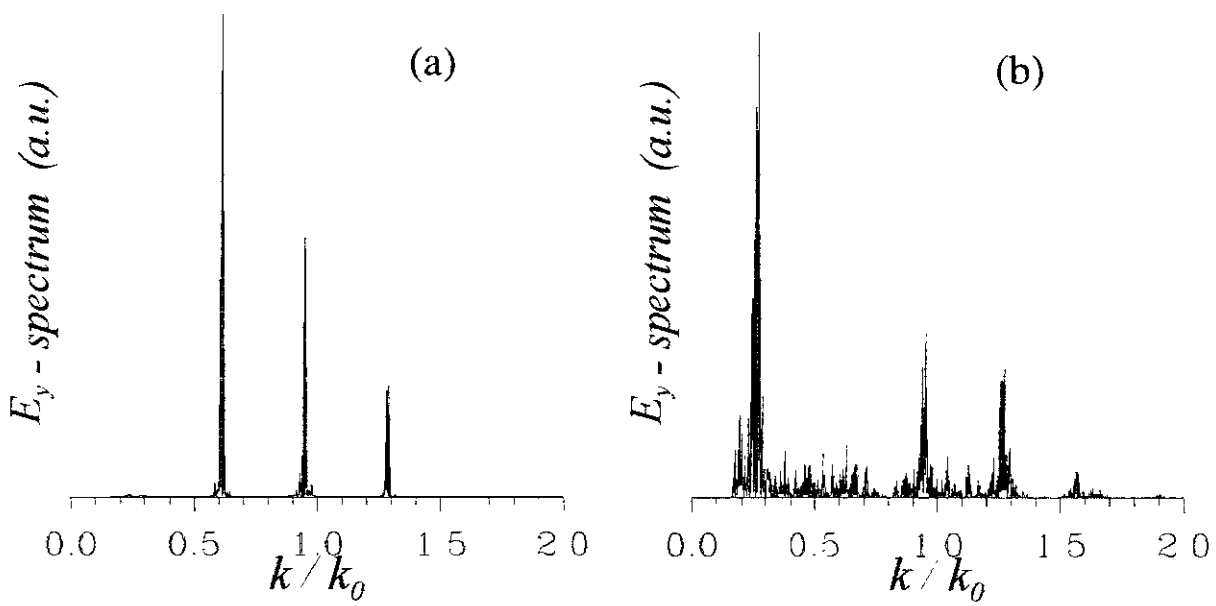

Figure 11.

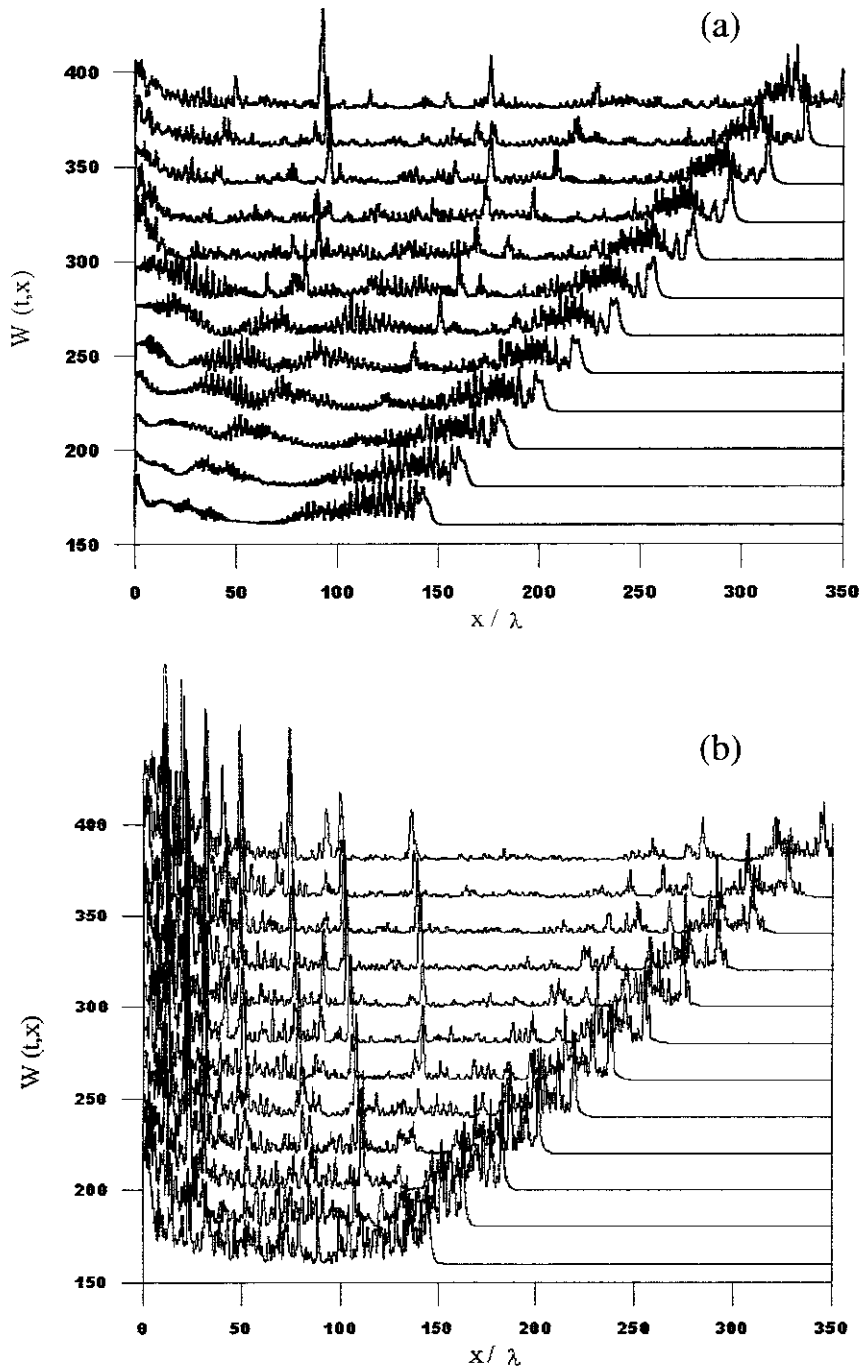
(a)
400
350
300
250
200
150
W (t,x)
0
50
100
150
200
250
300
350
x / λ
(b)
400
350
300
250
200
150
W (t,x)
0
50
100
150
200
250
300
350
x/ λ

Figure 12.

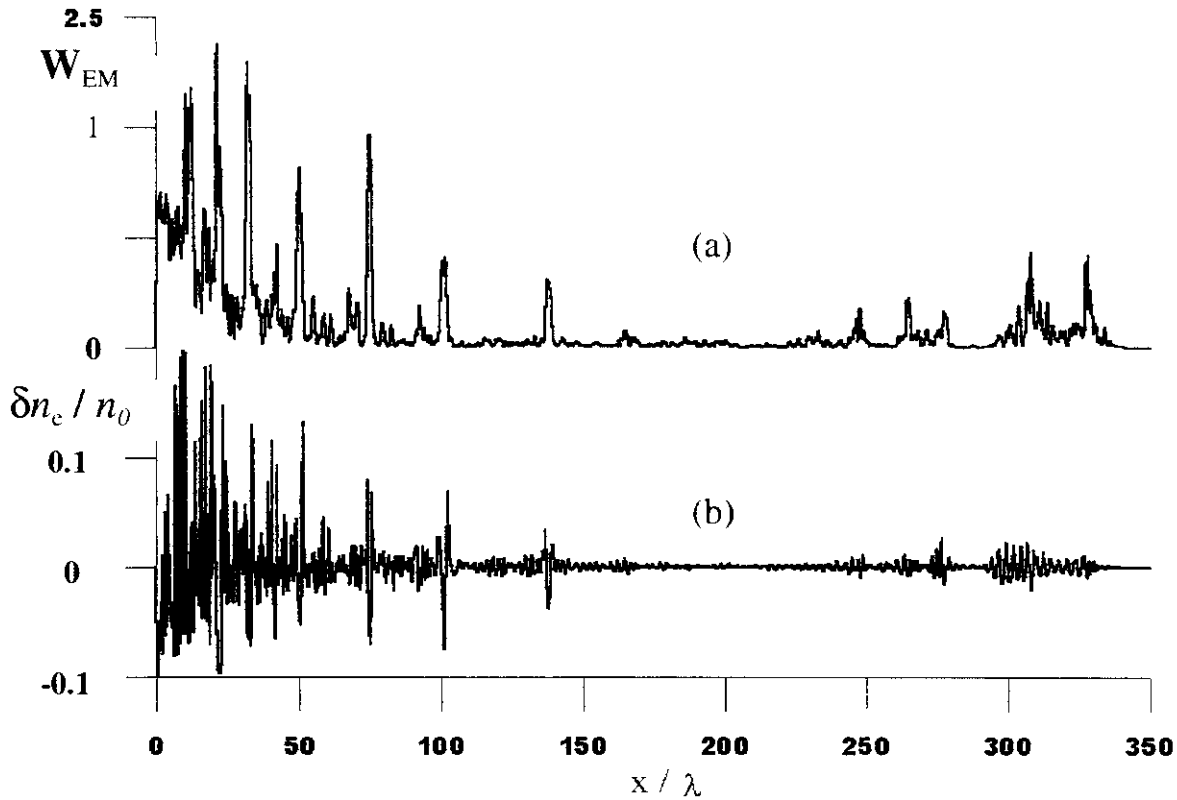

Figure 13.

Recent Issues of NIFS Series

NIFS-656 K Narihara, I Yamada, N Ohyabu, K Y Watanabe, N Ashikawa, P C deVries, M Emoto, H Funaba, M Goto, K Ichiguchi, K Ida, H Idei, K Ikeda, S Inagaki, N Inoue, K Isobe, S Kado, O Kaneko, K Kawahata, K Khlopenkov, T Kobuchi, A Komori, S Kubo, R Kumazawa, Y Liang, T Masuzaki, T Minami, J Miyazawa, T Morisaki, S Morita, S Murakami, S Muto, T Mutoh, Y Nagayama, Y Nakamura, H Nakanishi, Y Narushima, K Nishimura, N Noda, T Notake, S Ohdachi, Y Oka, M Osakabe, S Ozaki, R O Pavlichenko, B J Peterson, A Sagara, K Saito, S Sakakibara, R Sakamoto, H Sasao, M Sasao, K Sato, M Sato, T Seki, T Shimozuma, C Shoji, H Suzuki, A Takayama, M Takechi, Y Takeiri, N Tamura, K Tanaka, K Toi, N Tokuzawa, Y Torii, K Tsumori, T Watari, H Yamada, S Yamaguchi, S Yamamoto, M Yokoyama, Y Yoshimura, S Satow, K Itoh, K Ohkubo, K Yamazaki, S Sudo, O Motojima, Y Hamada, M Fujiwara
Transition from Ion Root to Electron Root in NBI Heated Plasmas in LHD Sep 2000
(IAEA-CN-77/EXP5/28)

NIFS-657 M Sasao, S Murakami, M Isobe, A V Krasilnikov, S Iiduka, K Itoh, N Nakajima, M Osakabe, K Saito, T Seki, Y Takeiri, T Watari, N Ashikawa, P deVaries, M Emoto, H Funaba, M Goto, K Ida, H Idei, K Ikeda, S Inagaki, N Inoue, S Kado, O Kaneko, K Kawahata, K Khlopenkov, T Kobuchi, A Komori, S Kubo, R Kumazawa, S Masuzaki, T Minami, J Miyazawa, T Morisaki, S Morita, S Muto, T Mutoh, Y Nagayama, Y Nakamura, H Nakanishi, K Narihara, K Nishimura, N Noda, T Notake, Y Liang, S Ohdachi, N Ohyabu, Y Oka, T Ozaki, R O Pavlichenko, B J Peterson, A Sagara, S Sakakibara, R Sakamoto, H Sasao4, K Sato, M Sato, T Shimozuma, M Shoji, H Suzuki, M Takechi, N Tamura, K Tanaka, K Toi, T Tokuzawa, Y Torii, K Tsumori, H Yamada, I Yamada, S Yamaguchi, S Yamamoto, M Yokoyama, Y Yoshimura, K Y Watanabe and O Motojima
Study of Energetic Ion Transport in the Large Helical Device Sep 2000
(IAEA-CN-77/EX9/1)

NIFS-658 B J Peterson, Y Nakamura, K Yamazaki, N Noda, J Rice, Y Takeiri, M Goto, K Narihara, K Tanaka, K Sato, S Masuzaki, S Sakakibara, K Ida, H Funaba, M Shoji, M Osakabe, M Sato, Yuhong Xu, T Kobuchi, N Ashikawa, P deVries, M Emoto, H Idei, K Ikeda, S Inagaki, N Inoue, M Isobe, S Kado, K Khlopenkov, S Kubo, R Kumazawa, T Minami, J Miyazawa, T Morisaki, S Murakami, S Muto, T Mutoh, Y Nagayama, H Nakanishi, K Nishimura, T Notake, Y Liang, S Ohdachi, Y Oka, T Ozaki, R O Pavlichenko, A Sagara, K Saito, R Sakamoto, H Sasao, M Sasao, T Seki, T Shimozuma, H Suzuki, M Takechi, N Tamura, K Toi, T Tokuzawa, Y Torii, K Tsumori, I Yamada, S Yamaguchi, S Yamamoto, M Yokoyama, Y Yoshimura, K Y Watanabe, T Watari, K Kawahata, O Kaneko, N Ohyabu, H Yamada, A Komori, S Sudo, O Motojima
Impurity transport induced oscillations in LHD Sep 2000
(IAEA-CN-77/EXP5/27)

NIFS-659 T Satow, S Imagawa, N Yanagi, K Takahata, T Mito, S Yamada, H Chikaraishi, A Nishimura, I Ohtake, Y Nakamura, S Satoh, O Motojima,
Achieved Capability of the Superconducting Magnet system for the Large Helical Device Sep 2000
(IAEA-CN-77/FTP1/15)

NIFS-660 T Watari, T Mutoh, R Kumazawa, T Seki, K Saito, Y Torii, Y P Zhao, D Hartmann, H Idei, S Kubo, K Ohkubo, M Sato, T Shimozuma, Y Yoshimura, K Ikeda, O Kaneko, Y Oka, M Osakabe, Y Takeiri, K Tsumori, N Ashikawa, P C deVries, M Emoto, A Fukuyama, H Funaba, M Goto, K Ida, S Inagaki, N Inoue, M Isobe, K Itoh, S Kado, K Kawahata, T Kobuchi, K Khlopenkov, A Komori, A Krasilnikov, Y Liang, S Masuzaki, K Matsuoka, T Minami, J Miyazawa, T Morisaki, S Morita, S Murakami, S Muto, Y Nagayama, Y Nakamura, H Nakanishi, K Narihara, K Nishimura, N Noda, A TNotake, S Ohdachi, N Ohyabu, H Okada, M Okamoto, T Ozaki, R O Pavlichenko, B J Peterson, A Sagara, S Sakakibara, R Sakamoto, H Sasao, M Sasao, K Sato, S Satoh, T Satow, M Shoji, S Sudo, H Suzuki, M Takechi, N Tamura, S Tanahashi, K Tanaka, K Toi, T Tokuzawa, K Y Watanabe, T Watanabe, H Yamada, I Yamada, S Yamaguchi, S Yamamoto, K Yamazaki, M Yokoyama, Y Hamada, O Motojima, M Fujiwara
The Performance of ICRF Heated Plasmas in LHD Sep 2000
(IAEA-CN-77/EX8/4)

NIFS-661 K Yamazaki, K Y Watanabe, A Sagara, H Yamada, S Sakakibara, K Narihara, K Tanaka, M Osakabe, K Nishimura, O Motojima, M Fujiwara, the LHD Group,
Helical Reactor Design Studies Based on New Confinement Scalings Sep 2000
(IAEA-CN-77/ FTP 2/12)

NIFS-662 T Hayashi, N Mizuguchi, H Miura and T Sato,
Dynamics of Relaxation Phenomena in Spherical Tokamak Sep 2000
(IAEA-CN-77THP2/13)

NIFS-663 H Nakamura and T Sato, H Kambe and K Sawada and T Saiki,
Design and Optimization of Tapered Structure of Near-field Fiber Probe Based on FDTD Simulation Oct 2000

NIFS-664 N Nakajima,
Three Dimensional Ideal MHD Stability Analysis in $L=2$ Heliotron Systems Oct 2000

NIFS-665 S Fujiwara and T Sato
Structure Formation of a Single Polymer Chain I Growth of trans Domains Nov 2000

NIFS-666 S Kida,
Vortical Structure of Turbulence Nov 2000

NIFS-667 H Nakamura S Fujiwara and T Sato,
Rigidity of Orientationally Ordered Domains of Short Chain Molecules Nov 2000

NIFS-668 T Mutoh, R Kumazawa, T Seki, K Saito, Y Torii, F Shimpo, G Nomura, T Watari, D A Hartmann, M Yokota, K Akaishi, N Ashikawa, P deVries, M Emoto, H Funaba, M Goto, K Ida, H Idei, K Ikeda, S Inagaki, N Inoue, M Isobe, O Kaneko, K Kawahata, A Komori, T Kobuchi, S Kubo, S Masuzaki, T Morisaki, S Morita, J Miyazawa, S Murakami, T Minami, S Muto, Y Nagayama, Y Nakamura, H Nakanishi, K Narihara, N Noda, K Nishimura, K Ohkubo, N Ohyabu, S Ohdachi, Y Oka, M Osakabe, T Ozaki, B J Peterson, A. Sagara, N Sato, S Sakakibara, R Sakamoto, H Sasao, M Sasao, M Sato, T Shimozuma, M Shoji, S Sudo, H Suzuki, Y Takeiri, K Tanaka, K Toi, T Tokuzawa, K Tsumori, K Y Watanabe, T Watanabe, H Yamada, I Yamada, S Yamaguchi, K Yamazaki, M Yokoyama, Y Yoshimura, Y Hamada, O Motojima, M Fujiwara
Fast- and Slow-Wave Heating of Ion Cyclotron Range of Frequencies in the Large Helical Device Nov 2000

NIFS-669 K Mima, M S Jovanovic, Y Sentoku, Z-M Sheng, M M Skoric and T Sato,
Stimulated Photon Cascade and Condensate in Relativistic Laser-plasma Interaction Nov 2000